

# Characterisation of multi-level quantum coherence without ideal measurements

Benjamin Dive<sup>1,2,3</sup>, Nikolaos Koukoulekidis<sup>1,2</sup>, Stefanos Mousafeiris<sup>2</sup>, and Florian Mintert<sup>2</sup>

<sup>1</sup>These two authors contributed equally to this work

<sup>2</sup>Department of Physics, Imperial College, London SW7 2AZ, UK

<sup>3</sup>Institute of Quantum Optics and Quantum Information, Austrian Academy of Sciences, Vienna 1090, Austria

December 15, 2024

**Coherent superpositions are one of the hallmarks of quantum mechanics and are vital for any quantum mechanical device to outperform the classically achievable. Generically, superpositions are verified in interference experiments, but despite their longstanding central role we know very little about how to extract the number of coherently superposed amplitudes from a general interference pattern. A fundamental issue is that performing a phase-sensitive measurement is as challenging as creating a coherent superposition, so that assuming a perfectly implemented measurement for verification of quantum coherence is hard to justify. In order to overcome this issue, we construct a coherence certifier derived from simple statistical properties of an interference pattern, such that any imperfection in the measurement can never over-estimate the number of coherently superposed amplitudes. We numerically test how robust this measure is to under-estimating the coherence in the case of imperfect state preparation or measurement, and find it to be very resilient in both cases.**

## 1 Introduction

The superposition principle allows wave mechanics, in particular quantum mechanics, to feature dynamics that are unthinkable for classical particles. The prospect of exploiting quantum coherence for applications in quantum computation, communication, metrology, and thermodynamics [1–5] has resulted in numerous activities towards the classification and quantification of quantum

coherence [6–13].

Those developments are strongly inspired by earlier work in the theory of entanglement. There is, however, a central difference between entanglement and coherence that poses a fundamental challenge in its experimental characterisation. To create entanglement it is necessary to use coherent interactions between particles that go beyond Local Operations and Classical Communications (LOCC). It can however be detected using only local measurements and classical processing of the resulting data, e.g., in terms of Bell inequalities, witnesses or state tomography [14, 15]. Thus, verifying entanglement requires less challenging experimental tools than to prepare it.

This distinction between resources needed for preparation and detection does not typically exist for coherence. Coherence is always defined with respect to a basis and this is generically the only basis in which measurements can be performed. Creating coherence requires an operation that maps a basis state into a coherent superposition of basis states; detecting coherence requires a measurement in such a superposition basis. As the latter typically cannot be done, it is instead replaced with an operation that maps the state back to an incoherent one (essentially the reverse of the preparation step), followed by a projection onto one of the basis states. This results in the awkward situation that any measurement that is supposed to verify the successful preparation of a coherent superposition is reliable only under the assumption that coherent superpositions can be created.

As we show here, this is not an insurmountable obstacle. We can find suitable figures of merit that offer a detailed characterisation of coherence properties, but that do not require any assump-

tion on the ability to realise operations that can create coherent superpositions.

Doing this first requires a rigorous definition of the aspects of coherence that we want to certify. For any given reference basis  $\{|j\rangle\}$ , one can define pure states  $|\Psi\rangle = \sum_j \psi_j |j\rangle$  with at least  $k$  non-vanishing amplitudes  $\psi_j$  to be  $k$ -coherent. Extending this, a mixed state  $\rho$  is  $k$ -coherent if all decompositions  $\rho = \sum_i p_i |\psi_i\rangle\langle\psi_i|$  into pure states  $|\psi_i\rangle$  with  $p_i \geq 0$  contains at least one  $k$ -coherent pure state [6]. Following this definition, the concept of  $k$ -coherence is closely analogous to genuine  $k$ -partite entanglement. Most of the prior literature on quantum coherence has not yet addressed this fine classification of different classes of coherence, but there are figures of merit that characterize  $k$ -coherence quantitatively [6, 16] or qualitatively [9]. To the best of our knowledge all existing approaches do rely on the assumption that measurements in a basis that is different to the preferred basis can be performed reliably. Our method does not require this and we focus on distinguishing incoherent states from those made up of at least 2, 3, or more basis states; it can also be applied to differentiate between higher values of  $k$ .

Here, we envision an experiment similar to the famous Ramsey sequence. This involves a preparation unitary  $U_p$  such that  $U_p |0\rangle = \sum_j \psi_j |j\rangle = |\psi\rangle$ , followed by an evolution  $U(t)$  generated by the system Hamiltonian  $H$  for a time  $t$ . This is followed by an effective projection onto a state  $|\chi\rangle = \sum_j \chi_j |j\rangle$  which is realised by the unitary evolution  $U_r$ , defined by  $U_r^\dagger |0\rangle = |\chi\rangle$ , and a subsequent projection onto the basis state  $|0\rangle$ . As such, the probability of getting a ‘click’ in the detector for an initial pure state  $|0\rangle$  is given by  $P(t) = |\langle\chi|U(t)|\psi\rangle|^2$ . This defines the interference pattern that is observed.

The coherence of  $|\psi\rangle$ , with respect to the eigenbasis of  $H$ , can be characterised in terms of the statistical moments of this probability distribution,  $M_q = \langle P^q \rangle$ , where the average is taken over the period of the dynamics. Under the promise that  $|\chi\rangle$  is a balanced superposition of all states of the reference basis, these moments provide a rigorous indicator of  $k$ -coherence. That is, there is a threshold value such that moments above this threshold value can only be achieved with states that are at least  $k$ -coherent [9]. The intuition behind this is that the interference pattern of

higher coherent states exhibit higher peaks and deeper troughs than low coherent states; in an analogous way to how the interference pattern of a diffraction grating and a double slit differ. This behaviour can be detected with the statistical moments, with higher moments being more sensitive to the more extreme peaks and troughs.

As argued above, it is highly problematic to assume that the desired projection onto the state  $|\chi\rangle$  can be performed reliably. Assuming that such a projection was performed when a different measurement was realised can suggest a higher degree of coherence than there is. This can easily be seen with the extreme case of  $|\chi\rangle = |0\rangle$ . In this case  $P(t)$  is maximised with the incoherent initial state  $|0\rangle$ , and since this holds for all  $t$ , also all moments adopt their maximum value for this state. Erroneously implementing a measurement including the projection onto the state  $|0\rangle$  rather than the projection onto a balanced superposition of all basis states is certainly not a realistic experimental scenario, but it helps to illustrate that uncontrollable experimental imperfections can result in wrong conclusions if assumptions on the type of measurement are made. In order to have trusted certification without making assumptions about the measurement we require a function that can identify coherence in the case of suitable measurements, but that does not result in false positives under flawed measurements.

In this paper we introduce a family of functions which do this, based on the ratio of moments of an interference pattern. We will show that those are convex functions of a quantum state, which makes them directly applicable to mixed states. The maximum value that such functions can adopt for a  $k$ -coherent state will be shown to be bounded from above independent of the Hamiltonian  $H$  and the projector  $|\chi\rangle\langle\chi|$ . Experimental limitations in the realization of the desired measurement will thus not result in wrong conclusions on the coherence properties of the state, but will in the worst case only result in the failure to exceed the threshold.

The construction of these coherence certifiers is presented in Sec.2, where their properties are also discussed. The technical aspects of the proofs are left to the appendices. In the cases where the exact threshold values are not known, we use numerical methods to approximate them; a discussion of these results is given in Sec.3. This

is followed in Sec.4 by a discussion of the ability of the proposed framework to verify  $k$ -coherence in the presence of various imperfections, and we conclude in Sec.5.

## 2 Coherence certifier

To talk in precise terms about the coherence certifiers we introduce, it is necessary to specify exactly the range of systems under consideration. The coherence of a state is defined with respect to a basis, and the natural basis to use for a Ramsey-like experiment is the eigenbasis of the system Hamiltonian. We make no restrictions on this Hamiltonian other than it being time-independent and having a discrete and commensurate spectrum (all finite Hamiltonians are discrete and  $\epsilon$ -close to being commensurate). It may contain some degeneracies but, as degenerate levels always have the same relative phases, these will never get picked up by the interference pattern and so the amount of coherence would be underestimated. As we are only lower bounding the coherence, this is not a problem. In order to simplify the analysis it is therefore convenient to ignore these degeneracies and, furthermore, expand the Hilbert space of the system by adding new levels such that the spectrum of the Hamiltonian is equally spaced. As this does not affect the evolution of the physical state, there is no loss of generality in only considering Hamiltonians

$$H = \sum_{n=1} n |n\rangle \langle n| , \quad (1)$$

with the spectrum of a harmonic oscillator.

As discussed in the introduction, the basic objects we use to study coherence are the moments of the interference pattern. The  $n^{\text{th}}$  moment is

$$\begin{aligned} M_n(\rho, |\chi\rangle) &= \frac{1}{2\pi} \int_0^{2\pi} p(t)^n dt \\ &= \frac{1}{2\pi} \int_0^{2\pi} \langle \chi | e^{-iHt} \rho e^{iHt} | \chi \rangle^n dt, \end{aligned} \quad (2)$$

where the duration of the integral is due to the energy scale picked in Eq.(1). The key object of interest is the ratio

$$R_n = \frac{M_n}{M_1^{n-1}} \quad (3)$$

of the moments  $M_n$  and  $M_1^{n-1}$  for  $n > 2$ . In particular, we will focus on  $R_3$  as it is the lowest order which can act as a coherence certifier.

$k$ -coherence	$R_3$ Threshold	$R_3$ Best Known
1	1	1
2	5/4	1.25
3	179/96 $\approx$ 1.86	1.77

Table 1: The maximum values that  $R_3$  can attain, for any rank-1 projector under any Hamiltonian, as a function of the  $k$ -coherence of the state. As such, exceeding these values means that the state must be at least  $(k+1)$ -coherent. The middle column is an upper bound to this highest value obtained analytically. The last column is the highest value we found after conducting a thorough numerical optimisation.

A central property of these functions is their convexity under the mixing of states

$$R_n(\lambda\rho_1 + (1-\lambda)\rho_2) \leq \lambda R_n(\rho_1) + (1-\lambda)R_n(\rho_2) \quad (4)$$

as proven in App.A. As coherence itself is convex, it is highly desirable for our certifier to also have this property. It implies that the maxima of  $R_n$  are adopted for pure states, so that threshold values found for pure states also apply to mixed states directly.

Another useful feature of  $R_n$  is that its maximum (for a state with fixed  $k$ -coherence) is reached when  $\rho = |\chi\rangle \langle \chi|$ . This is not necessary for a coherence certifier, but is nevertheless desirable for two reasons. Firstly it aligns with the intuition of a Ramsey-like interferometer, where the highest contrast is obtained by projecting onto the initial state, which is also what was found in prior work where  $|\chi\rangle$  was assumed to be the equal superposition state [9]. Secondly it further simplifies calculating the threshold values, rather than maximising over the  $4d$  real variables that define  $|\psi\rangle$  and  $|\chi\rangle$ : it is enough to consider only the  $d$  variables,  $\psi_i \chi_i^*$ , which can always be chosen such that they are real. This is proved in App.B.

Of particular interest is the need for  $R_n$  to be hierarchical, such that it can be used as a certifier. We have proved that  $R_3$  has a maximum value for fixed  $k$ , and have found an upper bound for this maximum, for  $k$ -coherent states for  $k = 1, 2, 3$  in App.C, using an analytic method that can generalise. Measuring a higher value than those thresholds, given in Tab.(1), therefore proves that the state is at least 2, 3, or 4-coherent respectively. In other cases it is strongly supported by numerical evidence discussed in Sec.3.

The assumption so far is that the measurement is projective; this can be relaxed. Consider the situation that a signal on the measurement device does not reliably indicate projection onto the state  $|\chi\rangle$ , but rather projection onto one of several states  $|\chi_j\rangle$  with probability  $q_j$ . This could happen if a different  $U_r$  is realised when the experiment is repeated to collect the statistics necessary to determine  $P(t)$ . In this case the recorded interference pattern reads

$$p(t) = \sum_j q_j p_j(t), \quad \text{where} \quad (5)$$

$$p_j(t) = \langle \chi_j | U(t) \rho U^\dagger(t) | \chi_j \rangle. \quad (6)$$

In exactly the same way that  $R_n$  is convex in its argument  $\rho$  for any given  $\chi$ , it is also convex in the second argument for any given  $\rho$  such that

$$\frac{\langle p(t)^n \rangle}{\langle p(t) \rangle^{n-1}} \geq \sum_j q_j \frac{\langle p_j(t)^n \rangle}{\langle p_j(t) \rangle^{n-1}}. \quad (7)$$

The results discussed so far therefore also apply to experimental imperfections resulting in fluctuations in the realisation of the projection.

### 3 Numerical threshold values

Although a general method to calculate an upper bound for the threshold values for  $R_3$  is given in App.C, this method is not easy to apply to large dimensions and it is therefore practical to find numerical values for the threshold. We do this by maximising the value of  $R_n$  over all states and measurements (for moderate values of  $n$  and  $k$ ), using the results of the previous section to simplify this problem. We are confident that the results found this way are an excellent approximation of the true maxima as it is stable under different parametrisation of the problem and for different initial conditions in the numerical optimisation. These numerical results can also be compared to the upper bounds given by the analytic results, thereby indicating how tight they are.

These numerical results are listed in Tab.(2), which also shows the state  $|\Psi_k\rangle$  that gives the maximum value of  $R_n$ , and how this value compares to the value given by the equally balanced state  $|W_k\rangle = \frac{1}{\sqrt{k}} \sum_i^k |i\rangle$ . A surprising point is that this equal superposition state is not the one which maximises  $R_n$ , a state with a larger population in the middle of the spectrum is preferred

$R_n$	$k$	$R_n( \Psi_k\rangle)$	$R_n( W_k\rangle)$	$\Psi_k$
$R_3$	2	1.25	1.25	(0.50, 0.50)
	3	1.77	1.74	(0.31, 0.38, 0.31)
	4	2.32	2.27	(0.22, 0.28, 0.28, 0.22)
	5	2.88	2.80	(0.17, 0.21, 0.23, 0.21, 0.17)
$R_4$	2	2.19	2.19	(0.50, 0.50)
	3	4.61	4.56	(0.32, 0.36, 0.32)
	4	8.02	7.90	(0.23, 0.27, 0.27, 0.23)
	5	12.42	12.21	(0.18, 0.21, 0.22, 0.21, 0.18)
$R_5$	2	3.94	3.94	(0.50, 0.50)
	3	12.39	12.28	(0.32, 0.36, 0.32)
	4	28.71	28.39	(0.24, 0.26, 0.26, 0.24)
	5	55.52	54.84	(0.19, 0.21, 0.21, 0.21, 0.19)

Table 2: Numerical results for the first three hierarchical ratios for up to 5-coherent states; showing their behaviour as coherence certifiers. The values of  $R_n$  are given for the equal superposition state  $|W_k\rangle$ , and for the state  $|\Psi_k\rangle$  which maximises the value, in all cases the projection is along the same state as it is known that this gives the highest value.  $|\Psi_k\rangle$  is found through numerical optimisation and is stable through different parametrisations of the problem and from different initial points, thereby making us confident that it lies very close to the true maximum. The amplitudes squared of  $|\Psi_k\rangle$  are also listed as a vector to show how it differs from the uniform case of  $\frac{1}{k}$ .

instead. One way to understand this is to note that interferences between basis states with small energy differences contribute more to  $R_n$  than those with large energy differences. As the basis states in the middle of the spectrum are closer to the rest of the basis states, the function is maximised by populating them more than the others. This intuition is more visible in the reparametrisation of  $R_n$  done in App.C. Furthermore, the larger  $n$  and  $k$  are, the more pronounced the difference between  $|W_k\rangle$  and  $|\Psi_k\rangle$  is.

In all cases of interest, however, the difference in the  $R_n$  value between  $|\Psi_k\rangle$  and  $|W_k\rangle$  is relatively small, which can be seen in Fig.(1). This figure also compares these to the analytic thresholds which shows how tight they are. Furthermore, the maximal values grow linearly (tested

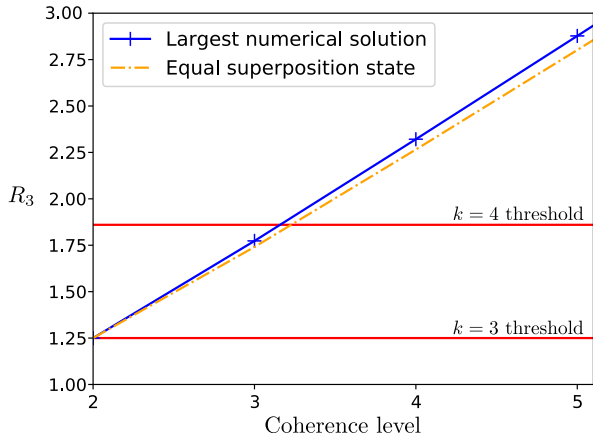


Figure 1: Comparison of numerical and analytical threshold values. The crosses show the maximum value that we found for  $R_3$  for states of difference coherence. The solid blue line is a linear fit for these, showing how they are equally spaced. The dashed orange line shows what value the equal superposition state  $|W_k\rangle$  has for the optimal measurement for comparison. The horizontal lines are the analytic threshold values. For the 2-coherent case, the equal superposition and optimal states overlap, and lie immediately below the threshold for certifying 3-coherence. For the 3-coherent case and higher, there is a finite but small gap between the equally balanced and optimal states. The threshold for 4-coherence also does not lie exactly above the maximum for 3-coherence, but the gap is again very small and, as we are lower bounding the amount of coherence present, this only means that  $R_3$  is occasionally too cautious about certifying states as highly coherent.

up to  $k = 30$ , not shown on the graph). This constant interval means that  $R_3$  would also be able to distinguish more highly coherent states. The functions  $R_4$  and  $R_5$  seem to have even faster growth, potentially making them more useful in such circumstances, although the additional experimental difficulty in accurately reconstructing higher moments should not be neglected [?].

## 4 Verification of $k$ -coherence in the presence of imperfections

In this section we demonstrate that our approach can verify coherence properties, even in the presence of substantial imperfections in the projective measurement and that coherence can also be detected in states with a rather high degree of mixing.

### 4.1 Measurement tolerance

As stated in the introduction, it is not always justified to assume that the projection can be performed perfectly in exactly the right direction. While we have already proved that an imperfect measurement will never overestimate the coherence of a state, it is also important that it does not underestimate it too strongly either. Therefore, we quantify this implication of measurement imperfections here. To achieve this, we produce a sample of random faulty measurement projections and estimate the deviation from perfect measurement required to reduce the value of the maximum  $k$ -coherent state below the  $k$ -coherence witness threshold.

In order to produce the sample of random measurements, we propagate the measurement operator which is initially at the maximum of  $k$ -coherence with a unitary  $\mathcal{U}$ ,

$$|\chi_k\rangle \mapsto \mathcal{U}(\tau) |\chi_k\rangle := e^{iH_r\tau} |\chi_k\rangle. \quad (8)$$

The parameter  $\tau$  is varied until the value of the ratio  $R_n(|\Psi_k\rangle\langle\Psi_k|, \mathcal{U}(\tau) |\chi_k\rangle)$  crosses the  $k$ -coherence witness threshold, so that the ratio can no longer distinguish  $k$ -coherence. The propagation is generated by a random Hamiltonian that belongs in the Gaussian Unitary Ensemble (GUE) [17], so that it is Hermitian and invariant under time reversal symmetry ( $\tau \rightarrow -\tau$ ). This ensures that the unitary propagator is not biased by the reference basis, which is always the Hamiltonian spectrum. We quantify the measurement deviation by the norm

$$\|\mathcal{U} |\chi_k\rangle - |\chi_k\rangle\| \equiv \sum_{i=1}^d [\mathcal{U}_{ij}\chi_j - \chi_i]^2. \quad (9)$$

A small value of the parameter  $\tau$  generates a small error in the projective measurement. The process is depicted in Fig.(2) for  $R_3$  and coherence levels  $k = 3$  and 4. Curves are initialised at the maximum over 3- and 4-coherent states, which correspond to ratio values of approximately 1.77 and 2.32 respectively according to Tab.(2), and drop towards the immediately lower coherent bound ( $= 1.25$  and 1.77 in Tab.(2)). The tolerance  $\mathcal{T}$  of  $R_3$  is the normed difference between the initial state and the state that crosses the threshold in the range  $[0, 2] \ni \tau$ . Some states are robust enough under imperfections in the projection, that they do not cross

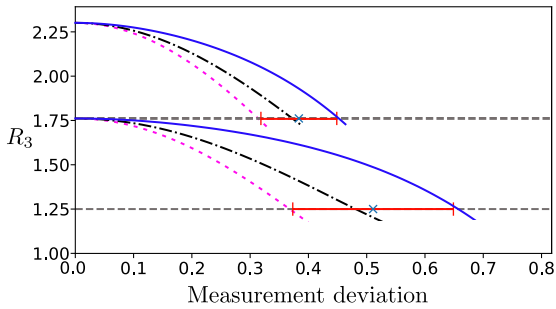


Figure 2:  $R_3$  value at the maximum system state against the normed difference of the initial measurement projector from the faulty one, for  $\tau \in [0, 2]$  and the transitions between coherence levels  $4 \rightarrow 3$  and  $3 \rightarrow 2$ . The crosses and error bars on the threshold lines indicate the mean tolerance  $\mathcal{T}$  and its standard deviation  $\sigma_{\mathcal{T}}$ . The curves plotted correspond to the mean value  $\mathcal{T}$  and  $\pm 1\sigma_{\mathcal{T}}$ .

the lower threshold in this range. In Fig.(2), the two black dotted lines indicate the interpolated average behaviour of a generated sample of 100 Hamiltonians, while the other lines represent Hamiltonians which cross one standard deviation  $\sigma_{\mathcal{T}}$  away from the average.

It is clear that the average tolerance increases for lower dimensional states, which is true for  $k > 4$  as well. Generally, (a ratio of higher order  $n \geq 4$  is) ratios  $R_4$  and  $R_5$  are observed to be even more tolerant in measurement deviations than  $R_3$  for a given coherence level  $k$ .

## 4.2 Decoherence tolerance

Since our central aim is the ability to verify coherence in the presence of experimental imperfections, the big remaining question is on the degree of decoherence that can be present, before our criteria fail to verify a desired level of coherence.

We explore the impact of decoherence by introducing the Werner-like state [18]

$$\rho_W = (1 - \lambda) |W_k\rangle \langle W_k| + \frac{\lambda}{k} \mathbb{I}_k, \quad (10)$$

and exploring the ability of the ratios to distinguish its level of coherence. The Werner-like state is a mixture of a maximally  $k$ -coherent and totally incoherent state. The degree of mixedness is varied with the parameter  $\lambda \in [0, 1]$ . When  $\lambda = 0$ , the system is a pure maximally-coherent state, while  $\lambda = 1$  corresponds to a mixed totally incoherent state respectively. Therefore, there must be a theoretical upper bound  $\lambda_{\text{dec}}$  above which the system is  $(k - 1)$  but not  $k$ -coherent.

Before reaching the bound, as  $\lambda$  increases from 0, it firstly reaches the threshold  $\lambda_{\text{patt}}$  at which an interference pattern can no longer distinguish  $k$ -coherence on the system. This is strongly dependent on the measurement projection that is applied. A projection onto an incoherent state clearly cannot distinguish any coherence on the system. Since ratios use no further knowledge about the system state than what the interference pattern provides, the threshold  $\lambda_{\text{thr}}$  at which they can distinguish  $k$ -coherence from lower coherence, can never be higher than  $\lambda_{\text{patt}}$ . These relations are illustrated in the following inequality,

$$0 < \lambda_{\text{thr}} \leq \lambda_{\text{patt}} \leq \lambda_{\text{dec}} < 1. \quad (11)$$

Ideally, the thresholds for ratio and pattern ability to identify  $k$ -coherence would coincide with the theoretical bound.

The bound at which  $\rho_W$  is at most  $q$ -coherent, with  $q \leq k$ , can be derived analytically,

$$\lambda_{\text{dec}} = \frac{k - q}{k - 1}, \quad 2 \leq q \leq k. \quad (12)$$

This is proved in App.D and this threshold is also discussed in Ref.[16]. This bound indicates that a state is never  $(q + 1)$ -coherent for any  $\lambda \geq \lambda_{\text{dec}}$ . The equality in the bound of  $\lambda$  holds whenever the system is maximally  $q$ -coherent. In summary,  $\rho_W$  is  $q$ -coherent if and only if  $\lambda < \frac{k - q + 1}{k - 1}$  for  $2 \leq q \leq k$ . The state is incoherent only at  $\lambda = 1$  and coherence level increases by 1 as  $\lambda$  increases in steps of  $\frac{1}{k - 1}$ . It is thus easier to distinguish maximal levels of coherence in low-dimensional spaces, which constitute the majority of experiments.

We can also show that optimisation of the measurement projection can bring the pattern threshold  $\lambda_{\text{patt}}$  arbitrarily close to  $\lambda_{\text{dec}}$ . This is a significant result because it implies that an interference pattern can provide enough information to identify the highest coherence level of the system in the presence of an arbitrary amount of decoherence. The proof that  $\lambda_{\text{patt}}$  can equal  $\lambda_{\text{dec}}$  for  $2 \leq q \leq k$  is also given in App.D.

For  $\lambda \geq \lambda_{\text{patt}}$ , a  $q$ -coherent state produces a pattern which can be decomposed into patterns that correspond to states of lesser coherence. In the case of an imperfect measurement projection, the value  $\lambda_{\text{patt}}$  drops away from  $\lambda_{\text{dec}}$  and therefore the pattern can be falsely decomposed for lower values of  $\lambda$  than it is possible in the case of

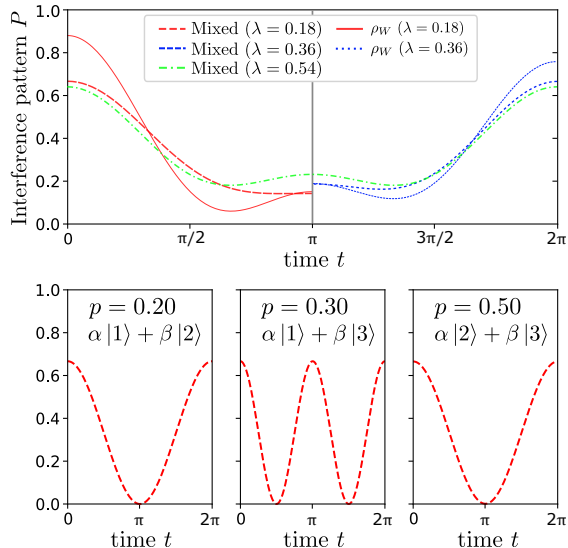


Figure 3: Interference patterns of  $\rho_W$  with different values of  $\lambda$  projected under ideal measurement. The state is 3-coherent and it cannot be decomposed into a mixture of 2-coherent states for  $\lambda < \lambda_{dec} = \frac{1}{2}$  as seen for the red and blue patterns ( $\lambda = 0.18, 0.36$  respectively). The solid/dotted curves represent the patterns arising from the projection of the 3-coherent Werner-like state  $\rho_W$ , while the dashed curves represent the optimal approximation of a mixed 2-coherent system. The green pattern corresponds to  $\lambda > \frac{1}{2}$ , so the two curves coincide, because the system can be theoretically decomposed. The bottom plots present three linearly independent 2-coherent states that, when mixed optimally, with the shown mixture probabilities  $p$ , they approximate but do not match the pattern of  $\rho_W$  at  $\lambda = 0.18$ . The  $R_3$  values of the states are, 1.26, 0.88, 0.60, with increasing  $\lambda$ , so the system corresponding to the red curve can be certified by  $R_3$  as 3-coherent.

perfect projection. Significant deviations of measurement projection from  $\lambda_{dec}$  result in inability to verify the highest coherence level present in the system.

In Fig.(3), three interference patterns of the 3-coherent Werner-like state are plotted along with approximate decompositions of the states into a mixture of 2-coherent states. As long as  $\lambda < \lambda_{dec} = \frac{1}{2}$ , which is the case for the red and blue curves (corresponding to  $\lambda = 0.18, 0.36$  respectively), the state is seen to not decompose into states of lower coherence under ideal measurement, as expected by the result that the pattern has a threshold value equal to the theoretical  $\lambda_{dec}$ . The green pattern ( $\lambda = 0.54$ ) coincides with its decomposition, because  $\lambda > \lambda_{dec}$  in this case. If the measurements were sufficiently far from the

$k$	3	4	5	6	7	8	9	10
$R_3$	0.18	0.13	0.10	0.08	0.06	0.06	0.05	0.04
$R_4$	0.28	0.19	0.14	0.11	0.09	0.08	0.07	0.06
$R_5$	0.33	0.22	0.16	0.13	0.11	0.09	0.08	0.07

Table 3: Decoherence thresholds  $\lambda_{thr}$  for  $R_3, R_4$  and  $R_5$  between consecutive levels of coherence for  $k = 3$  to 10.

optimal, the patterns to the red and blue systems would be decomposable into patterns of 2-coherent states. The red pattern corresponds to  $R_3(\rho_W(\lambda = 0.18)) = 1.26 > \max_{k=2} R_3$ , and so it is detectable by our coherence certifier. Its approximate decomposition which minimises vertical distance from the pattern is given on the bottom part of the plot. It is a mixture of three 2-coherent states, which is the minimum number of basis states required to form the 3-dimensional Werner-like state. For  $\lambda > \frac{2}{3}$ , the patterns could also be decomposed simply into incoherent states, as Eq.(12) indicates.

The threshold  $\lambda_{thr}$  at which the ratios can no longer distinguish the highest level of coherence is then found numerically and presented for  $R_3, R_4$  and  $R_5$  at the first coherence levels in Tab.(3). As coherence level increases, the ratio threshold and the theoretical  $k$ -coherence bound get closer to each other for all ratios  $R_3, R_4$  etc. However, they tend to zero, meaning that coherence is more easily detectable at low level systems, as expected. We also find that ratios  $R_n$  of higher  $n$  result in higher numerical thresholds which are even closer to the ideal value  $\lambda_{dec}$ , as seen in Tab.(3) for  $R_4$  and  $R_5$ .

## 5 Conclusion

Despite the numerous similarities between the theories of entanglement and coherence, the equality in operation required for creation and verification of quantum coherence defines a crucial difference between those two theories. Our proposed solution relies on easily observable quantities such that an imperfectly implemented verification protocol can never overestimate the degree of coherence. As such, it offers very practical and robust avenue to rigorously verify coherence properties beyond the two-level setting.

Beyond the fundamental question ‘when is a triple-slit interference pattern so washed out, that

one can not recognize it anymore?”, the ability to verify the number of states contributing to a coherent superposition has also very practical applications in the verification that a potential quantum device is actually able to operate in the quantum regime that it is supposed to.

## 6 Acknowledgments

We are grateful for stimulating discussions with Nicky Kai Hong Ling, and for his contributions. B.D. acknowledges funding from the Engineering and Physical Sciences Research Council (EPSRC UK) administered by Imperial College London via the Postdoctoral Prize Fellowship program for the core duration of this work; and funding from the Österreichische Akademie Der Wissenschaften via FWF-Project P 30947 for the closing stages. N.K. acknowledges funding from the EPSRC UK through the Controlled Quantum Dynamics Centre for Doctoral Training for the closing stages.

## References

- [1] D. Stahlke, *Physical Review A* **90**, 022302 (2014).
- [2] E. Knill, R. Laflamme, and G. Milburn, [arXiv:quant-ph/0006088](https://arxiv.org/abs/quant-ph/0006088) (2000).
- [3] C. Zhang, B. Yadin, Z. B. Hou, H. Cao, B. H. Liu, Y. F. Huang, R. Maity, V. Vedral, C. F. Li, G. C. Guo, and D. Girolami, *Physical Review A* **96**, 1 (2017).
- [4] M. Lostaglio, K. Korzekwa, D. Jennings, and T. Rudolph, *Physical Review X* **5**, 021001 (2015).
- [5] K. Korzekwa, M. Lostaglio, J. Oppenheim, and D. Jennings, *New Journal of Physics* **18**, 023045 (2016).
- [6] F. Levi and F. Mintert, *New Journal of Physics* **16**, 033007 (2014).
- [7] T. Baumgratz, M. Cramer, and M. B. Plenio, *Physical Review Letters* **113**, 140401 (2014).
- [8] D. Girolami, *Physical Review Letters* **113**, 170401 (2014).
- [9] K. Von Prillwitz, A. Rudnicki, and F. Mintert, *Physical Review A* **92**, 052114 (2015).
- [10] A. Winter and D. Yang, *Physical Review Letters* **116**, 120404 (2016).
- [11] I. Marvian and R. W. Spekkens, *Physical Review A* **94**, 052324 (2016).
- [12] A. Streltsov, U. Singh, H. S. Dhar, M. N. Bera, and G. Adesso, *Physical Review Letters* **115**, 020403 (2015).
- [13] A. Streltsov, G. Adesso, and M. B. Plenio, *Reviews of Modern Physics* **89**, 041003 (2017).
- [14] R. Horodecki, M. Horodecki, and K. Horodecki, *Reviews of Modern Physics* **81**, 865 (2009).
- [15] N. Friis, G. Vitagliano, M. Malik, and M. Huber, *Nature Reviews Physics* (2018).
- [16] M. Ringbauer, T. R. Bromley, M. Cianciaruso, S. Lau, G. Adesso, A. G. White, A. Fedrizzi, and M. Piani, *Physical Review X* **8**, 41007 (2017).
- [17] Y. V. Fyodorov, [arXiv:math-ph/0412017](https://arxiv.org/abs/math-ph/0412017) (2004).
- [18] R. F. Werner, *Phys. Rev. A* **40**, 4277 (1989).
- [19] R. A. Horn and C. R. Johnson, *Matrix Analysis* (Cambridge University Press, 1985).
- [20] M. Nath Bera, T. Qureshi, M. Asad Siddiqui, and A. K. Pati, *Physical Review A* **92**, 012118 (2015).

## A Proof that $R_n$ is convex

To prove that  $R_n$  is convex under the mixing of states we need to show that

$$R_n(\lambda\rho_1 + (1-\lambda)\rho_2) \leq \lambda R_n(\rho_1) + (1-\lambda)R_n(\rho_2), \quad (13)$$

for all pairs of states  $\rho_1, \rho_2$ , for all  $\lambda \in [0, 1]$ , and for any choice of projector  $|\chi\rangle$ . This property holds for the moment themselves, which are convex and positive by construction. Products and sums of such functions stay convex, but this is not necessarily the case for ratios of them. We prove that this particular function is indeed convex, for  $n \geq 2$ , by taking the second derivative of Eq.(13) with respect to  $\lambda$  and showing that it is always non-negative.

This second derivative is

$$\partial_\lambda^2 R_n = \frac{M_1^{3n-5}}{M_1^{4n-4}} [M_1^2 \partial_\lambda^2 M_n - 2(n-1)M_1(\partial_\lambda M_1)\partial_\lambda M_n + n(n-1)(\partial_\lambda M_1)^2 M_n].$$

Denoting the kernel of  $M_n$  in Eq.(2) by  $p^n$  and the time average by  $\langle \cdot \rangle$ , allows the derivatives to be calculated according to

$$\begin{aligned} \partial_\lambda M_n &= \langle n(\partial_\lambda p)p^{n-1} \rangle, \\ \partial_\lambda^2 M_n &= \langle n(n-1)(\partial_\lambda p)^2 p^{n-2} \rangle. \end{aligned}$$

Substituting these expressions into Eq.(14) gives

$$\partial_\lambda^2 R_n = \frac{M_1^{3n-5}}{M_1^{4n-4}} \langle n(n-1)p^{n-2} [p\langle \partial_\lambda p \rangle - \langle p \rangle \partial_\lambda p]^2 \rangle, \quad (14)$$

where the fraction at the front is non-negative, as is the squared term in the time average and its pre-factor (for  $n \geq 2$ ), thereby showing that  $R_n$  is convex as desired.

## B Proof that $R_n$ is maximised for equal preparation and projection

We begin by noting that the expression for the probability distribution in Eq.(2) for pure states is given by the double sum

$$p(t) = \sum_{p,q} \chi_p^* \psi_p \psi_q^* \chi_q e^{-i(p-q)t}, \quad (15)$$

where the subscripts denote the matrix components in the basis of  $H$  and the spectrum is taken from Eq.(1). By defining  $\psi_p \chi_p^* = \alpha_p e^{i\phi_p}$ ,  $\phi_{pq} = \phi_p - \phi_q$  and  $\omega_{pq} = p - q$  this can be recast as

$$p(t) = \sum_p \alpha_p^2 + 2 \sum_{p>q} \alpha_p \alpha_q \cos(\omega_{pq}t + \phi_{pq}), \quad (16)$$

where the  $\alpha$  are real and non-negative by construction.

We now show that the maximum is reached when the phases  $\phi_{pq}$  are all zero. Firstly, because integrating cosines over an integer number of periods gives nothing the first moment is independent of them

$$M_1 = \sum_p \alpha_p^2. \quad (17)$$

It is therefore clear that changes in  $\phi_{pq}$  (arising from different phases between the state and the projector) affect the numerator of  $R_n$  but not the denominator. The terms of  $M_{>1}$  which depend non-trivially on the phases are inside the integral over time and are of the form

$$\int_0^{2\pi} \left( \sum_{p>q} \alpha_p \alpha_q \cos(\omega_{pq}t + \phi_{pq}) \right)^m dt. \quad (18)$$

To see which terms do not vanish when integrated over, it is useful to look at the products of cosines individually

$$\int_0^{2\pi} \alpha_{p_1} \alpha_{q_1} \cos(\omega_{p_1 q_1} t + \phi_{p_1 q_1}) \times \alpha_{p_2} \alpha_{q_2} \cos(\omega_{p_2 q_2} t + \phi_{p_2 q_2}) \times \dots dt. \quad (19)$$

which can themselves be expanded into a sum of cosines, where each term is of the form

$$\propto \int_0^{2\pi} \cos[(\omega_{p_1 q_1} \pm \omega_{p_2 q_2} \dots)t + \phi_{p_1 q_1} \pm \phi_{p_2 q_2} \dots]. \quad (20)$$

If the sum (for the different permutations of signs) of frequencies do not sum to 0, then the integral vanishes. If they do sum to 0, the term is proportional to the cosine of the sum (for the different permutations of signs) of the phases. One of the solutions which maximises this is to pick all the  $\phi_{pq} = 0$ , which simultaneously maximises every such integral no matter the number of terms or the sign configuration. This itself increases  $M_n$  and therefore the value of  $R_n$ .

In this case that there are no relative phases,  $R_n$  can be written in terms of a simplified Eq.(16) as

$$R_n = \frac{\int_0^{2\pi} \left( \sum_p \alpha_p^2 + 2 \sum_{p>q} \alpha_p \alpha_q \cos(\omega_{pq} t) \right)^n}{\left( \sum_p \alpha_p^2 \right)^{n-1}}. \quad (21)$$

From this it can be seen that the mapping  $\alpha_p \rightarrow x \alpha_p$  changes the function  $R_n \rightarrow x^2 R_n$ . It is therefore desirable to make  $\alpha$  as large as possible. From Cauchy-Schwarz we have an upper bound on increasing the  $\alpha$  according to

$$\begin{aligned} \left( \sum_p \alpha_p \right)^2 &= \left( \sum_p \psi_p \chi_p \right)^2 \\ &\leq \left( \sum_p \psi_p \right)^2 \left( \sum_p \chi_p \right)^2 = 1, \end{aligned} \quad (22)$$

thereby limiting their sum to 1. Therefore, in the case that  $\sum \alpha_p = A \leq 1$ , the value of  $R_n$  can be increased by instead choosing  $\alpha'_p = \alpha_p A^{-1}$ . There always exist a normalised state  $|\psi\rangle$  and measurement basis  $|\chi\rangle$  which satisfy this while both being normalised, namely,  $\psi_k = \chi_k = \sqrt{\alpha_p A^{-1}}$ . Indeed, from Cauchy-Schwarz, the only choice of  $|\psi\rangle$  and  $|\chi\rangle$  which lead to  $\sum \alpha_p = 1$  is when  $|\psi\rangle = |\chi\rangle$ .

This condition is equivalent to saying that, at the maximum value of  $R_n$  for a fixed  $k$ -coherence, the input state is pure and identical to the projective measurement. Mathematically this is the requirement that in Eq.(21) the  $\alpha_i$  are all non-negative and sum to 1. Note that this is a slightly different statement to saying that for every pure state  $R_n$  is maximised by picking the same measurement as the state.

## C Derivation of analytic threshold values

The starting point is Eq.(21) and we now make another simplification in the notation by grouping together terms with the same frequency  $\omega_{pq} = p - q$ . This allows the sum over the cosines to be expressed as

$$\sum_{p>q} \alpha_p \alpha_q \cos(\omega_{pq} t) = \sum_n D_n \cos(\omega_n t) \quad (23)$$

where the new variables are given by

$$D_n = \sum_p \alpha_{p+n} \alpha_p, \quad \omega_n = p - q, \quad (24)$$

which also lets us rewrite the term  $\sum_p \alpha_p^2 = D_0$ , thereby unifying the notation. We also recall that, from previous arguments, that  $\sum_p \alpha_p = 1$  for the maximum of the function. Using this notation in Eq.(21) for the case  $n = 3$  we obtain

$$\begin{aligned} R_3 = \int_0^{2\pi} & \left[ D_0 + 6 \sum_i D_i \cos(\omega_i t) + \frac{12}{D_0} \sum_{ij} D_i D_j \cos(\omega_i t) \cos(\omega_j t) + \right. \\ & \left. \frac{8}{D_0^2} \sum_{ijk} D_i D_j D_k \cos(\omega_i t) \cos(\omega_j t) \cos(\omega_k t) \right] dt \end{aligned} \quad (25)$$

Performing the integrals in the way described earlier, only terms where the  $\omega$  sum to 0 contribute, which yields

$$\begin{aligned} R_3 &= 6D_0 \left( \frac{1}{6} + \sum_{ij} \frac{D_i D_j}{D_0^2} \delta_{ij} + \sum_{ijk} \frac{D_i D_j D_k}{D_0^3} \sigma_{ijk} \right) \\ &= D_0 \left( \frac{1}{6} + \sum_i \tilde{D}_i^2 + \sum_{ijk} \tilde{D}_i \tilde{D}_j \tilde{D}_k \sigma_{ijk} \right) \end{aligned} \quad (26)$$

where  $\sigma_{ijk}$  is a phase matching condition which is 1 if  $i + j = k$  and 0 otherwise, and  $\tilde{D}_i = \frac{D_i}{D_0}$ .

Finding the maximum value of  $R_3$  for fixed  $k$ -coherence has proved very difficult, but we have done it for low  $k$  here in a method which should generalise, although it may become too laborious to be practical. The key idea is to treat the  $\{\tilde{D}_i\}$  as independent variables to optimise over and  $D_0$  as a ‘free’ parameter. Eq.(24) is used to form linear constraints on the  $\{\tilde{D}_i\}$ , which forms an outer approximation to the physically allowed region for a choice of  $D_0$ . We then show that in this region  $R_3$  has a positive definite Jacobian, which implies that for any line cutting through this region, the maxima of the function must where the line crosses the bounding surface. Therefore, the maximum value is attained at one of the vertices. As this region is defined by linear constraints it is a polytope, and hence has only a finite number of vertices which can be individually evaluated to see which produces the largest value of  $R_3$ . The remaining step is then optimise over  $D_0$ , which is easily done numerically as the problem is reduced to finding the turning points of a quotient of low order polynomials in one dimension.

Although we could not show that the Jacobian is positive in general, we do find that it is in all the cases of interest. For convenience, it is useful to list its components here. These are the derivatives of  $R_3$ , which are given by

$$\partial_{\tilde{D}_a} R_3 = 6D_0 \left( 2D_a + 2 \sum_{jk} \tilde{D}_j \tilde{D}_k \sigma_{ajk} + \sum_{ij} \tilde{D}_i \tilde{D}_j \sigma_{ija} \right)$$

$$\partial_{\tilde{D}_a} \partial_{\tilde{D}_a} R_3 = 12D_0(1 + D_{2a}) \quad (27)$$

$$\partial_{\tilde{D}_b} \partial_{\tilde{D}_a} R_3 = 12D_0(D_{a+b} + D_{|a-b|}). \quad (28)$$

$$k = d = 3$$

We show in full detail how this method works for  $d = 3$ . Explicitly, we have as our variables:

$$D_0 = \alpha_1^2 + \alpha_2^2 + \alpha_3^2$$

$$D_1 = \alpha_1 \alpha_2 + \alpha_2 \alpha_3$$

$$D_2 = \alpha_1 \alpha_3$$

$$1 = \alpha_1 + \alpha_2 + \alpha_3.$$

From this we can write some inequalities which constrain the allowed values. Firstly, as the  $\alpha$ 's are all positive we have that  $0 \leq D_0$  and  $0 \leq \tilde{D}_i$ . Secondly, the triangle inequality implies that

$$\frac{1}{d} \leq D_0 \leq 1. \quad (29)$$

The first non-trivial constraint comes about from the same starting point

$$\begin{aligned} 1 &= (\alpha_1 + \alpha_2 + \alpha_3)^2 \\ &= D_0 + 2D_1 + 2D_2 \\ &= D_0 \left( 1 + 2 \sum_i \tilde{D}_i \right). \end{aligned} \quad (30)$$

From these two relations we upper bound the maximum values of any  $\tilde{D}_i$

$$\begin{aligned} \frac{1}{d} \left( 1 + 2 \sum_i \tilde{D}_i \right) &\leq 1 \\ \sum_i \tilde{D}_i &\leq \frac{d-1}{2} \\ \tilde{D}_i &\leq \frac{d-1}{2}. \end{aligned} \quad (31)$$

Other inequalities can be obtained by considering well chosen sums of squares, the three useful ones are listed here. Firstly

$$\begin{aligned}(\alpha_1 - \alpha_3)^2 + \alpha_2^2 &\geq 0 \\ D_0 - 2D_2 &\geq 0 \\ 1 - 2\tilde{D}_2 &\geq 0.\end{aligned}\tag{32}$$

Changing the sign gives a different inequality

$$\begin{aligned}(\alpha_1 + \alpha_3)^2 + \alpha_2^2 &\geq \frac{1}{2} \\ D_0 + 2D_2 &\geq \frac{1}{2} \\ D_0(1 + 2\tilde{D}_2) &\geq \frac{1}{2},\end{aligned}\tag{33}$$

where the triangle inequality is used in the first line. Lastly, there is

$$\begin{aligned}(\alpha_1 - \alpha_2 + \alpha_3)^2 &\geq 0 \\ D_0 - 2D_1 + 2D_2 &\geq 0 \\ 1 - 2\tilde{D}_1 + 2\tilde{D}_2 &\geq 0.\end{aligned}\tag{34}$$

The last three equations (for fixed  $D_0$ ) define a triangular region of interest, while Eq.(30) is a line that cuts through it. They can be expressed as succinctly as

$$\begin{aligned}\max\left(\frac{1-2D_0}{4D_0}, 0\right) &\leq \tilde{D}_2 \leq \frac{1}{2} \\ 0 \leq \tilde{D}_1 = \frac{1-D_0}{2D_0} - \tilde{D}_2 &\leq 1 \\ 0 \leq 1 - 2\tilde{D}_1 + 2\tilde{D}_2 &\end{aligned}\tag{35}$$

In order to be sure that the maxima of the function in this region is located at the vertices, we need the Jacobian, which is

$$\begin{pmatrix} 1 + D_2 & D_1 \\ D_1 & 1 \end{pmatrix},$$

which is strictly positive definite everywhere in the allowed region. Therefore, the only points that need to be examined are the vertices of the polytope (in this case, just a line) defined by Eq.(35) for the valid range of  $D_0$ . It therefore just remains to find these vertices by solving these equations on the boundary in the  $\tilde{D}_1 - \tilde{D}_2$  plane, which depends on the value of  $D_0$ . They can be summarised as

$\tilde{D}_1$	$\tilde{D}_2$	$D_0$	$\max R_3$
$\frac{1-D_0}{2D_0}$	0	$\frac{1}{2} \leq D_0 \leq 1$	1.25
$\frac{1-2D_0}{2D_0}$	$\frac{1}{2}$	$\frac{1}{3} \leq D_0 \leq \frac{1}{2}$	1.58
$\frac{1}{4D_0}$	$\frac{1-2D_0}{4D_0}$	$\frac{1}{3} \leq D_0 \leq \frac{1}{2}$	1.86

where the largest values of  $R_3$  over all  $D_0$  in the allowed range are also given. From this we can conclude that if  $R_3$  is larger than 1.86 we can certify that the state is not a 3-coherent state lying in adjacent energy levels of an SHO. For comparison, the perfectly balanced state gives 1.74 and the largest value we could find numerically was 1.77. The largest value found for a 4-coherent state (that we want to distinguish from) is 2.32, while for a 2-coherent state it is 1.25.

$$k = 3, d \geq 3$$

We now remove the restriction on the dimension and instead restrict ourselves to a 3-level state, which is to say that only 3 of the  $\alpha$ 's are non-zero. Without loss of generality, we have as the three populated levels  $1, p, q$  with  $1 < p < q$ . This means that the only non-zero variables are  $\alpha_1, \alpha_p, \alpha_q$ , which gives

$$D_0 = \alpha_1^2 + \alpha_p^2 + \alpha_q^2,\tag{36}$$

$$D_{p-1} = \alpha_1 \alpha_p,\tag{37}$$

$$D_{q-p} = \alpha_p \alpha_q,\tag{38}$$

$$D_{q-1} = \alpha_1 \alpha_q\tag{39}$$

with the assumption that  $p - 1 \neq q - p$ . If these are equal, then the energy levels are equally spaced and we are back to the 3-level case considered in the first instance. As usual, we now find inequalities on the  $\tilde{D}$ 's to define a volume. As each one only contains a single term, this can be done for each independently by considering

$$(\alpha_i - \alpha_j)^2 + \alpha_k^2 \geq 0 \quad (40)$$

$$(\alpha_i + \alpha_j)^2 + \alpha_k^2 \geq \frac{1}{2}, \quad (41)$$

where  $i, j, k$  are all different. This and results of Eqs.(29,30) gives

$$\max\left(0, \frac{1 - 2D_0}{4D_0}\right) \leq \tilde{D}_i \leq \frac{1}{2} \quad (42)$$

$$\frac{1}{3} \leq D_0 \leq 1 \quad (43)$$

$$\tilde{D}_{p-1} + \tilde{D}_{q-p} + \tilde{D}_{q-1} = \frac{1 - D_0}{2D_0}. \quad (44)$$

The first line defines a cube in  $\tilde{D}_i$  space and the last two a family of planes that cut through that space. We show that within the cube the Jacobian is always positive.

The function  $R_3$ , and therefore the Jacobian, depends on the indices of the  $\tilde{D}$  due to the  $\sigma$  “energy matching” term in the triple sum. There are several triplets that could enter:

$$D_{p-1} D_{q-p} D_{q-1} \quad (45)$$

always contributes

$$D_{p-1} D_{p-1} D_{q-1} \text{ or } D_{q-p} D_{q-p} D_{q-1} \quad (46)$$

are ruled out by the condition  $p - 1 \neq q - p$

$$D_{p-1} D_{p-1} D_{q-p} \quad (47)$$

if and only if  $q = 3p - 2$

$$D_{q-p} D_{q-p} D_{p-1} \quad (48)$$

if and only if  $q = \frac{1}{2}(3p - 1)$

The first case is the generic one. The second case happens if the energy differences are equal, which we explicitly rule out. The third case happens if the populated levels are  $(1, 2, 4), (1, 3, 7), \dots$  where the energy difference is in the ratio  $1 : 2$ . The third case requires the populated levels to be  $(1, 3, 4), (1, 5, 7), \dots$  where the energy difference has the ratio  $2 : 1$ . This is therefore identical to the previous case under the Hamiltonian mapping  $H \rightarrow -H$ , which clearly leaves the interference pattern unchanged.

There are thus 2 different cases to consider. The Jacobian in the first case is

$$\begin{pmatrix} 1 & \tilde{D}_{q-1} & \tilde{D}_{q-p} \\ \tilde{D}_{q-1} & 1 & \tilde{D}_{p-1} \\ \tilde{D}_{q-p} & \tilde{D}_{p-1} & 1 \end{pmatrix}. \quad (49)$$

This is positive definite as, from Eq.(44) all principle minors of the matrix are themselves positive definite in the cubic region of interest [19]. The second case has the Jacobian

$$\begin{pmatrix} 1 + \tilde{D}_{q-p} & \tilde{D}_{q-1} + \tilde{D}_{p-1} & \tilde{D}_{q-p} \\ \tilde{D}_{q-1} + \tilde{D}_{p-1} & 1 & \tilde{D}_{p-1} \\ \tilde{D}_{q-p} & \tilde{D}_{p-1} & 1 \end{pmatrix}, \quad (50)$$

which is also positive everywhere, except potentially at some of the vertices of the cube.

The vertices can be found in much the same way as before, except that the boundaries are now symmetric between the  $\tilde{D}_i$ . We therefore give them as triplets where all permutations need to be considered separately for evaluating  $R_3$ .

$D_0$	$\tilde{D}_i$	$\tilde{D}_j$	$\tilde{D}_k$	max $R_3$ (generic)	max $R_3$ (1 : 2 ratio)
$\frac{1}{2} < D_0 \leq 1$	0	0	$\frac{1 - D_0}{2D_0}$	1.25	1.25
$\frac{1}{3} \leq D_0 \leq \frac{1}{2}$	$\frac{1 - 2D_0}{4D_0}$	$\frac{1 - 2D_0}{4D_0}$	$\frac{1}{2}$	1.27	1.33

(51)

Importantly, these values are all lower than for the case of a 3-level system in adjacent energy levels. Therefore, the previous result we had is very significantly strengthened: if  $R_3$  is larger than 1.86 then we know that the state is not 3-coherent for any Hamiltonian.

$$k = d = 4$$

To highlight that this algorithmic way of calculating the threshold values can be extended to high dimensions, we demonstrate it for the case of 4-coherent states. In order to reduce the number of cases to consider, we limit ourselves to states where the 4 populated levels are all adjacent basis states of an harmonic Hamiltonian. For this case, the variables are

$$\begin{aligned} D_0 &= \alpha_1^2 + \alpha_2^2 + \alpha_3^2 + \alpha_4^2 \\ D_1 &= \alpha_1\alpha_2 + \alpha_2\alpha_3 + \alpha_3\alpha_4 \\ D_2 &= \alpha_1\alpha_3 + \alpha_2\alpha_4 \\ D_3 &= \alpha_1\alpha_4. \end{aligned}$$

Eqs.(29, 30, 31) hold as before. Other bounds can be obtained in a similar way to before by considering sums of squares. These are firstly

$$\begin{aligned} (\alpha_1 - \alpha_3)^2 + (\alpha_2 - \alpha_4)^2 &\geq 0 \\ 1 - 2\tilde{D}_2 &\geq 0, \end{aligned} \tag{52}$$

and

$$\begin{aligned} (\alpha_1 + \alpha_3)^2 + (\alpha_2 + \alpha_4)^2 &\geq \frac{1}{2} \\ D_0(1 + 2\tilde{D}_2) &\geq \frac{1}{2}. \end{aligned} \tag{53}$$

Similarly there is

$$\begin{aligned} (\alpha_1 - \alpha_4)^2 + \alpha_2^2 + \alpha_3^2 &\geq 0 \\ 1 - 2\tilde{D}_3 &\geq 0, \end{aligned} \tag{54}$$

and

$$\begin{aligned} (\alpha_1 + \alpha_4)^2 + \alpha_2^2 + \alpha_3^2 &\geq \frac{1}{3} \\ D_0(1 + 2\tilde{D}_3) &\geq \frac{1}{3}. \end{aligned} \tag{55}$$

Finally

$$\begin{aligned} (\alpha_1 - \alpha_2 + \alpha_3 - \alpha_4)^2 &\geq 0 \\ 1 - 2\tilde{D}_1 + 2\tilde{D}_2 - 2\tilde{D}_3 &\geq 0. \end{aligned} \tag{56}$$

Rougher versions of these can be obtained by eliminating  $D_0$  by taking the ‘worst case’ approach, providing the simple inequalities

$$\begin{aligned} \tilde{D}_1 &\leq 1 & \tilde{D}_1 + \tilde{D}_3 &\leq 1 \\ \tilde{D}_2 &\leq \frac{1}{2} & \tilde{D}_3 &\leq \frac{1}{2}, \end{aligned} \tag{57}$$

which will be useful in proving the positivity of the Jacobian. The Jacobian is given by

$$\begin{pmatrix} 1 + D_2 & D_1 + D_3 & D_2 \\ D_1 + D_3 & 1 & D_1 \\ D_2 & D_1 & 1 \end{pmatrix}. \tag{58}$$

The easiest way to prove positivity is, as before, to show that each of the principle minors is itself positive definite in [19], which is straightforward to compute in the region of interest defined by the inequalities Eq.(57). As before, it remains to find the vertices as a function of  $\tilde{D}_2$ . This is a harder problem than before, which is most easily tackled by rewriting the tighter inequalities as

$$\max\left(0, \frac{1 - 2D_0}{4D_0}\right) \leq \tilde{D}_2 \leq \frac{1}{2} \tag{59}$$

$$\max\left(0, \frac{1 - 3D_0}{6D_0}\right) \leq \tilde{D}_3 \leq \frac{1}{2} \tag{60}$$

$$0 \leq 1 - 2\tilde{D}_1 + 2\tilde{D}_2 - 2\tilde{D}_3 \tag{61}$$

$$0 \leq \tilde{D}_1 = \frac{1 - D_0}{2D_0} - \tilde{D}_2 - \tilde{D}_3 \leq 1 \tag{62}$$

The first two describe a surface in the  $\tilde{D}_2 - \tilde{D}_3$ , with the coordinates of the vertices depending on the value of  $D_0$ . The third equation states how this protrudes in the  $\tilde{D}_1$  direction. The fourth describes a plane that cuts this volume, and imposes additional physical constraints. The way to solve this is therefore, for a given range of  $D_0$ , to find the vertices in the  $\tilde{D}_2 - \tilde{D}_3$  plane (a maximum of 4), find the corresponding value of  $\tilde{D}_1$  and check if any additional constraints on  $D_0$  arise. The results are summarised below.

$D_0$	$\tilde{D}_1$	$\tilde{D}_2$	$\tilde{D}_3$	$\max R_3$
$\frac{1}{2} < D_0 \leq 1$	$\frac{1-D_0}{4D_0}$	0	0	1
$\frac{1}{3} < D_0 \leq \frac{1}{2}$	$\frac{1-2D_0}{2D_0}$	$\frac{1}{2}$	0	1.58
	$\frac{1-2D_0}{4D_0}$	$\frac{1-2D_0}{4D_0}$	$\frac{1}{2}$	1.25
	$\frac{1}{4D_0}$	$\frac{1-2D_0}{4D_0}$	0	1.86
$\frac{1}{4} \leq D_0 \leq \frac{1}{3}$	$\frac{1-3D_0}{2D_0}$	$\frac{1}{2}$	$\frac{1}{2}$	1.33
	$\frac{2-3D_0}{6D_0}$	$\frac{1}{2}$	$\frac{1-3D_0}{6D_0}$	2.44
	$\frac{1-2D_0}{4D_0}$	$\frac{1-2D_0}{4D_0}$	$\frac{1}{2}$	1.93

We see that the plane can intersect the volume at a single point (one vertex), in a plane (three vertices) or, in the case that  $D_0 = \frac{1}{4}$  in a line (two vertices). It is to be expected that this geometry becomes far more complicated in higher dimensions. This sort of analyses ought to generalise, but doing so is probably difficult. Nevertheless, from the table we can conclude that if  $R_3$  is larger than 2.44 we can certify that the state is not a 4-coherent state lying in adjacent energy levels of an SHO. For comparison, the perfectly balanced state gives 2.26 and the largest value we could find numerically was 2.32. The largest value found for a 5-coherent state (that we want to distinguish from) was 2.88.

## D Derivation of decoherence theoretical and pattern thresholds

We first derive the theoretical threshold of coherence for the state  $\rho_W$  and then prove that an interference pattern gives a threshold equal to the theoretical, under perfect measurement.

We observe that  $\rho_W$  is fully symmetric under permutations of basis states as well as that all the off-diagonal elements are  $\frac{1-\lambda}{k}$ , resulting in

$$C_{\ell_1}(\rho_W) = (k-1)(1-\lambda), \quad (64)$$

where  $C_{\ell_1}(\rho) = \sum_{i \neq j} |\rho_{ij}|$  is the  $\ell_1$ -norm as studied by Bera *et al* [20]. These two properties define a Werner-like state.

The  $\ell_1$  norm of a  $q$ -coherent state is bounded from above. The bound is obtained when the system state is pure since  $C_{\ell_1}$  is a convex measure [20]. Let  $\rho^{(q)} = |\alpha^{(q)}\rangle \langle \alpha^{(q)}|$  for a state  $\alpha^{(q)}$  defined in the reference basis, so that  $\rho_{ij} = \alpha_i \alpha_j^* = \alpha_i^* \alpha_j$  and  $\text{Tr}(\rho) = \sum_{i=1}^q |\rho_{ii}| = 1$ .

$$(q-1) - C_{\ell_1}(\rho^{(q)}) = (q-1) \sum_{i=1}^q |\rho_{ii}| - 2 \sum_{i < j} |\rho_{ij}| \quad (65)$$

$$= \sum_{j \neq i} \sum_{i=1}^q |\rho_{ii}| - 2 \sum_{i < j} |\rho_{ij}| \quad (66)$$

$$= \sum_{i < j} |\alpha_i|^2 - 2 \sum_{i < j} |\alpha_i| |\alpha_j| \quad (67)$$

$$= \sum_{i < j} (|\alpha_i| - |\alpha_j|)^2 \geq 0. \quad (68)$$

This means that the coherence of the system is bounded above,

$$C_{\ell_1}(\rho^{(q)}) \leq q-1, \quad (69)$$

with equality obtained when  $\forall i, j, |\alpha_i| = |\alpha_j|$  in the reference basis, so that  $|\alpha\rangle$  is the maximally  $q$ -coherent state.

Using Eqs.(64, 69), we obtain

$$\lambda \geq \frac{k-q}{k-1} \quad (70)$$

$$\therefore \lambda_{\text{dec}} = \frac{k-q}{k-1}, \quad 2 \leq q \leq k. \quad (71)$$

Now projecting with the ideal measurement we get

$$\Omega_k = \sum_{i=1}^k |\chi_i|^2 |\rho_{ii}| = \frac{1}{k} \sum_{i=1}^q |\rho_{ii}| = \frac{1}{k} \quad (72)$$

$$\forall i, j \quad r_{ij} = |\chi_i^* \chi_j \rho_{ij}| = \frac{1}{k} |\rho_{ij}| \quad (73)$$

$$\therefore P\left(\rho^{(q)}, |W_k\rangle, H, t\right) = \Omega_k + 2 \sum_{i < j} r_{ij} \cos(\omega_{ij}t + \phi_{ij}) \quad (74)$$

$$\leq \frac{1}{k} + \frac{2}{k} \sum_{i < j} |\rho_{ij}| = \frac{1}{k} + \frac{1}{k} C_{\ell_1}\left(\rho^{(q)}\right) \quad (75)$$

$$\leq \frac{1}{k} + \frac{q-1}{k} = \frac{q}{k} \quad (76)$$

Returning to our decoherence question, a pattern with a maximum higher than this boundary value,  $\frac{q-1}{k}$ , cannot be decomposed into patterns arising from coherence lower than  $q$ . We get the threshold value  $\lambda_{\text{patt}}$  at which the interference pattern can no longer distinguish consecutive coherence levels, by bounding the interference pattern produced from the Werner-like state by the probability maximum, so that

$$\begin{aligned} \frac{q}{k} &\geq \langle \chi_0 | \rho_k | \chi_0 \rangle = 1 - \lambda + \frac{\lambda}{k} \\ \lambda &\geq \frac{k-q}{k-1} \\ \therefore \lambda_{\text{patt}} &= \frac{k-q}{k-1}, \quad 2 \leq q \leq k, \end{aligned} \quad (77)$$

which coincides with  $\lambda_{\text{dec}}$  for  $q = k - 1$ .